NANO LETTERS

pubs.acs.org/NanoLett Letter

Scalable Integration of High Sensitivity Strain Sensors Based on Silicon Nanowire Spring Array Directly Grown on Flexible Polyimide Films

Xiaopan Song, Yang Gu, Sheng Wang,* Junyu Fan, Junyang An, Lei Yan, Bin Sun, Junzhuan Wang, and Linwei Yu*

Cite This: *Nano Lett.* 2025, 25, 2290−2297 Read Online

ACCESS | Metrics & More | Article Recommendations | Supporting Information

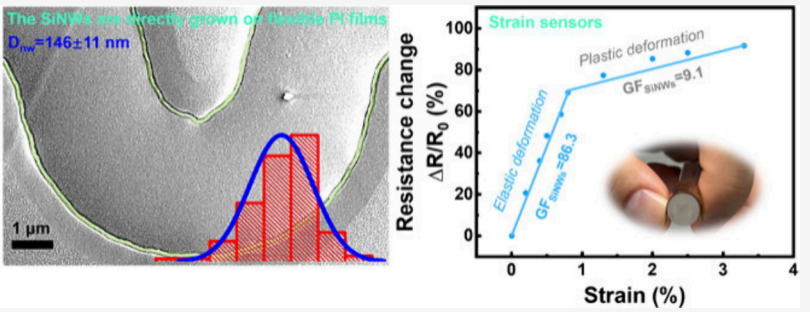

ABSTRACT: The growth and integration of position-controlled, morphology-programmable silicon nanowires (SiNWs), directly upon low-cost polymer substrates instead of postgrowth transferring, is attractive for developing advanced flexible sensors and logics. In this work, a low temperature growth of SiNWs at only 200 °C has been demonstrated, for the first time, upon flexible polyimide (PI) films, via a planar solid−liquid−solid (IPSLS) growth mechanism. The SiNWs with diameter of ∼146 nm can be grown into precise locations on PI as orderly array and with preferred elastic geometry. Strain sensor array, built upon these spring-shape SiNWs integrated on PI, achieves a gauge factor (GF) of ∼90, sustains large stretching strains up to 3.3% (with 1.5 mm radius) and endures over 30,000 cycles. Strain sensors attached to the finger to monitor movements are also successfully demonstrated, showing high sensitivity and superior mechanical reliability, particularly suited for wearable health applications.

KEYWORDS: *silicon nanowire growth, morphology-programmable, IPSLS, strain sensors, flexible electronics*

With the rapid development of wearable technology and flexible electronics, the demand for high-performance, reliable sensors is growing.[1−4] This is especially true in the fields of health monitoring, environmental surveillance, and intelligent living.[5−7] Particularly noteworthy are electronic skins (E-skins) that integrate various miniaturized devices on flexible/stretchable substrates for detecting ultrasmall strains.[8−10] These E-skins can conform closely to the epidermis, minimizing discomfort to the user, and have attracted widespread attention in recent years.[11] Flexible strain sensors are key components of E-skins.[12,13] On the one hand, skin deformation can reflect useful information about human movements and emotions, such as finger bending, swallowing, and heartbeats.[14−17] Real-time monitoring of strain distribution in E-skins can calibrate devices whose output signals may be significantly affected by strain. Developing reliable E-skins capable of detecting ultrasmall strains has significant research value. Organic thin films, commonly used for flexible strain sensing, are prepared by spin-coating or printing but often have lower stability compared to inorganic materials and require additional encapsulation layers for protection.[18−20]

Meanwhile, nanowire structures, such as metal or alloy nanowires, are widely used in flexible/stretchable strain sensing applications due to high flexibility and macroscopic lengths.[21−23] However, they typically have macroscopic widths or diameters, which limit their integration and application in ultrasmall strain sensing. Ideally, the sensing materials required in electronic skins should be as small as possible and preferably have a specific morphological structure to adapt to the changes in flexible substrates, meeting the requirements of high flexibility and high integration density. Additionally, inorganic silicon nanowires (SiNWs) structure is widely applied in flexible sensing areas due to high crystallinity, excellent mechanical properties, and superior electrical performance,

Received: November 6, 2024
Revised: January 24, 2025
Accepted: January 24, 2025
Published: January 30, 2025

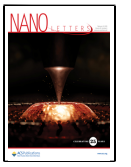

https://doi.org/10.1021/acs.nanolett.4c05553
Nano Lett. 2025, 25, 2290−2297

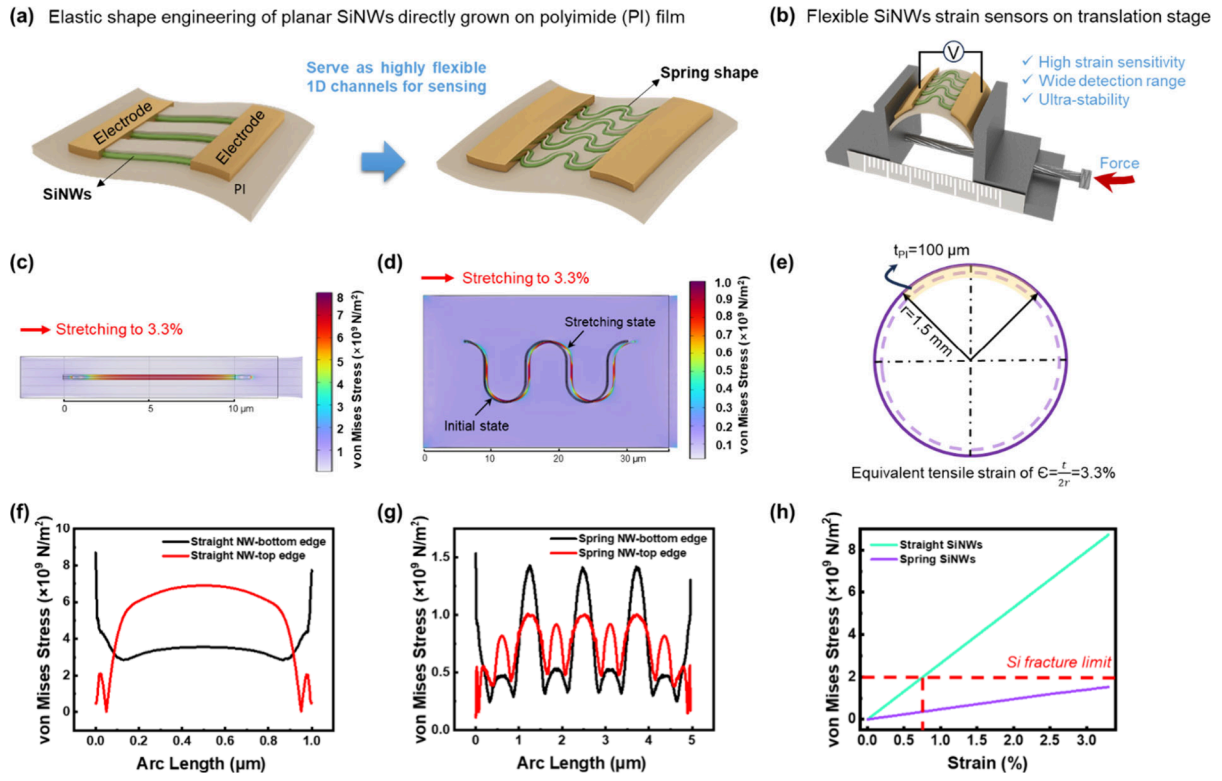

Figure 1. (a) Schematics of straight and spring-shaped SiNWs on a flexible PI substrate. (b) Spring-shaped sensor setup on a custom stretch platform. (c-d) Stress distribution in straight and spring-shaped SiNWs. (e) Conversion from convex bending to surface tensile strain, showing an equivalent stretch of 3.3%. (f-g) Stress distribution along the bottom and top of straight and spring NWs constrained by the PI film. (h) Max von Mises stress vs strain, highlighting the higher stress and earlier fracture risk in straight NWs compared to spring-shaped ones.

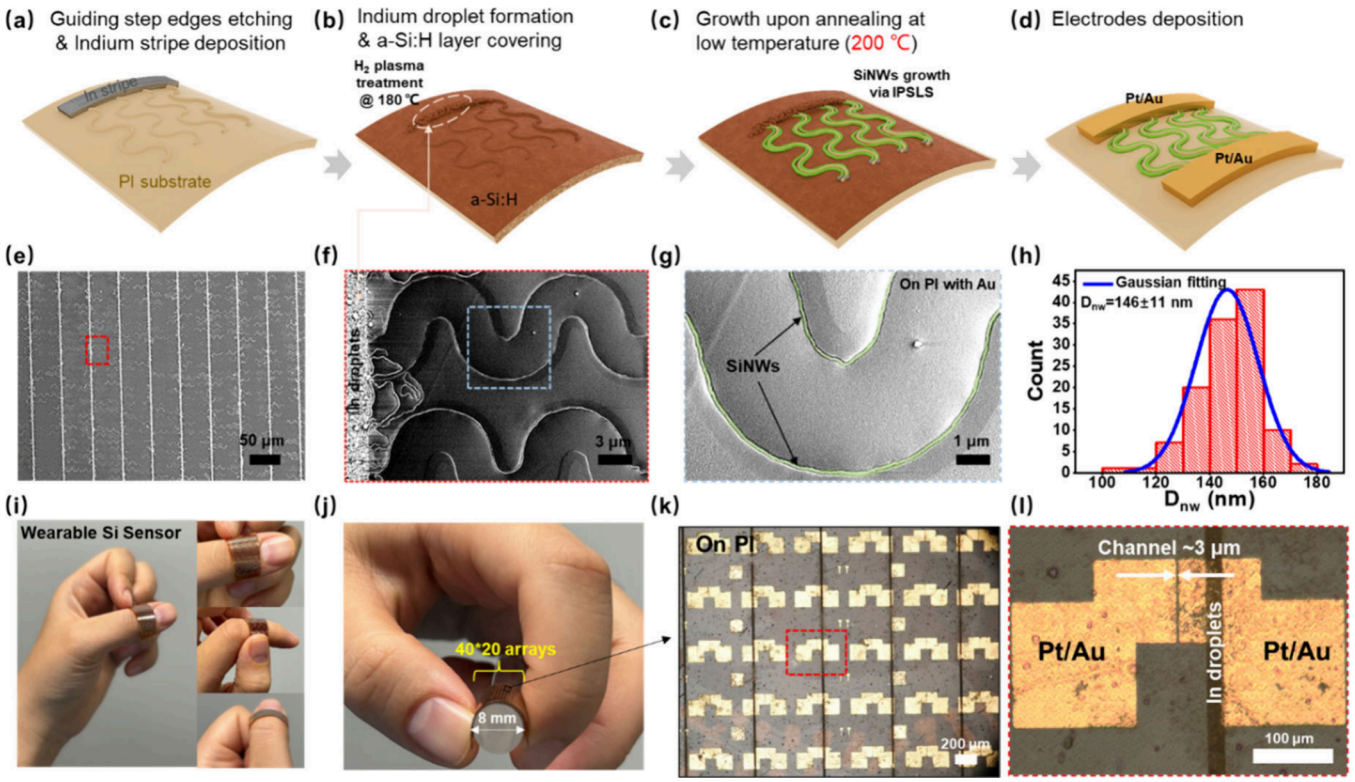

Figure 2. (a-d) Typical process for fabricating self-aligned spring-shaped SiNW arrays strain sensors on a flexible PI substrate. (e-g) SEM of spring-shaped NWs growing along step edges. (h) Diameter statistics. (i-j) Images of the flexible SiNW strain sensor array on a PI film attached to a human finger. Optical microscope images of the array are shown in (k-l).

https://doi.org/10.1021/acs.nanolett.4c05553
Nano Lett. 2025, 25, 2290−2297

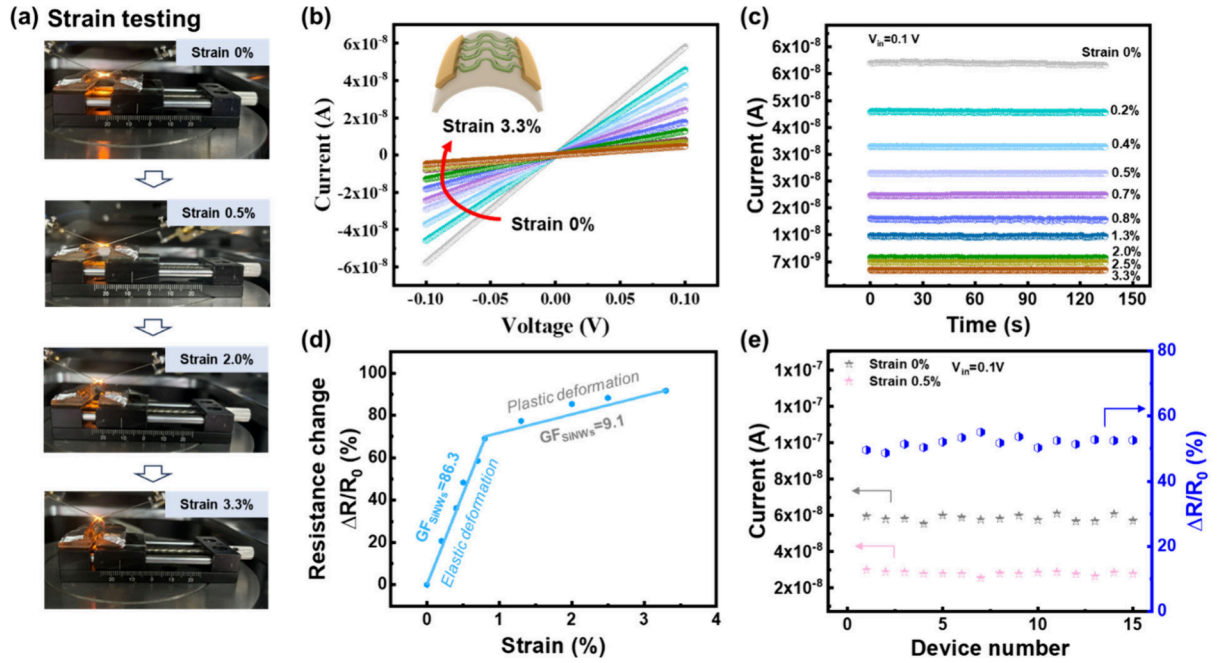

Figure 3. (a) Physical picture for the flexible SiNW strain sensor on a stretching platform. (b) Electrical characteristics during straining. inset: sensor schematic. (c) Time-dependent current changes under various strains at 0.1 V bias. (d) $\Delta R/R_0$ vs strain, with GF extracted for 0−0.8% and 0.8−3.3% strain ranges. (e) Current and resistance changes for 15 flexible strain sensors.

resulting in outstanding stability and robustness.[24−28] For example, flexible strain sensors prepared by transferring centimeter-long SiNW to a flexible substrate have achieved a strain sensitivity as high as 52.[29] Utilizing the contraction of elastic polymer substrates to force the attached SiNW into out-of-plane bending, forming stretchable SiNWs capable of enduring more than 45% strain and over 10,000 stretching cycles.[13] However, these SiNWs are typically grown by using traditional vapor−liquid−solid (VLS) methods and then transferred to flexible/stretchable substrates, which is difficult to precisely design the morphology and position of the NWs and to scale up the integration of flexible strain sensors.

To directly grow morphology-programmable and orderly SiNW on a flexible substrate, we developed a novel in-plane solid−liquid−solid (IPSLS) growth mechanism.[30−36] While highly ordered SiNWs have been demonstrated on hard substrates, their direct growth on a soft polyimide (PI) substrate and integration into high-performance strain sensor arrays have not been studied. In this work, we designed two types of the NWs (Figure 1a). Finite element analysis (FEA) simulations validated that spring-shaped NWs can withstand significant strain without breaking. The schematic of the flexible strain sensor fixed on a translation platform is shown in Figure 1b. The SiNWs experienced an equivalent tensile strain of 3.3% (Figure 1e). Stress simulations (Figure 1c-d) show higher stress at the bottom of straight-shaped NWs and at the peaks/troughs of spring-shaped NWs. Stress values (Figure 1f-g) reveal that straight NWs exhibit extremely high stress (up to 9 GPa) at the bottom edges, while spring-shaped NWs show stress spikes (∼1.5 GPa) at the bottom edges, peaking at the bending points. The straight-shaped NWs consistently exhibit higher stress than spring-shaped NWs (Figure 1h). Within the fracture strength limit of silicon (>2 GPa),[37−39] straight-shaped NWs may break under small strains (∼0.8%). This work reports a flexible strain sensor array based on spring-shaped NWs, with a maximum strain range of 3.3%, over 30,000 cycles, achieving a high gauge factor (GF) close to 90 (at 0.8% strain) and minimal hysteresis, providing a foundation for advanced flexible sensing and wearable electronics.

RESULTS AND DISCUSSION

As depicted in Figures 2a-d, spring-shaped SiNWs were grown on PI substrate, and fabricated into flexible strain sensors. Indium (In) stripes were defined and evaporated (Figure 2a). The sample was then loaded into a plasma-enhanced chemical vapor deposition (PECVD) system for hydrogen (H_2) plasma treatment. A film of a-Si precursor was deposited (Figure 2b), followed by a vacuum annealing at 200 °C that activates the In droplets to absorb the nearby a-Si and produces aligned SiNWs along the guiding edges (Figure 2c), Finally, the residual a-Si layer was selectively etched. Metal electrodes of Pt/Au were fabricated via electron beam evaporation (EBE) and lift-off procedure. Detailed experimental and growth mechanisms (Figure S1) were provided in the Supporting Information.

Figures 2e-g show typical field emission scanning electron microscopy (SEM) images of SiNWs grown along predefined spring morphological step edges on a PI substrate. The density of SiNWs at specified positions is extremely high. Magnified SEM images, colored green for clarity, reveal precisely oriented spring-shaped NWs with a diameter of D_{nw} = 146 ± 11 nm, as shown in the statistical data in Figure 2h. Figures 2i-j demonstrate a flexible SiNW strain sensor array attached to a human finger, showing that the device can conformally adhere to soft skin and remain intact even under arbitrary bending and squeezing. Optical microscope images in Figure 2k show an array of device units on a flexible PI substrate maintaining structural integrity without microcracks. The detailed device configuration, highlighted by the red dashed box in the enlarged view of Figure 2l, reveals electrodes and a channel region of L_{ch} ∼ 3 μm. Additionally, straight-shaped SiNW arrays can also grow on a flexible PI substrate, as shown in SEM images in Figure S2a-b, with a diameter of D_{nw} = 142 ± 9

https://doi.org/10.1021/acs.nanolett.4c05553
Nano Lett. 2025, 25, 2290−2297

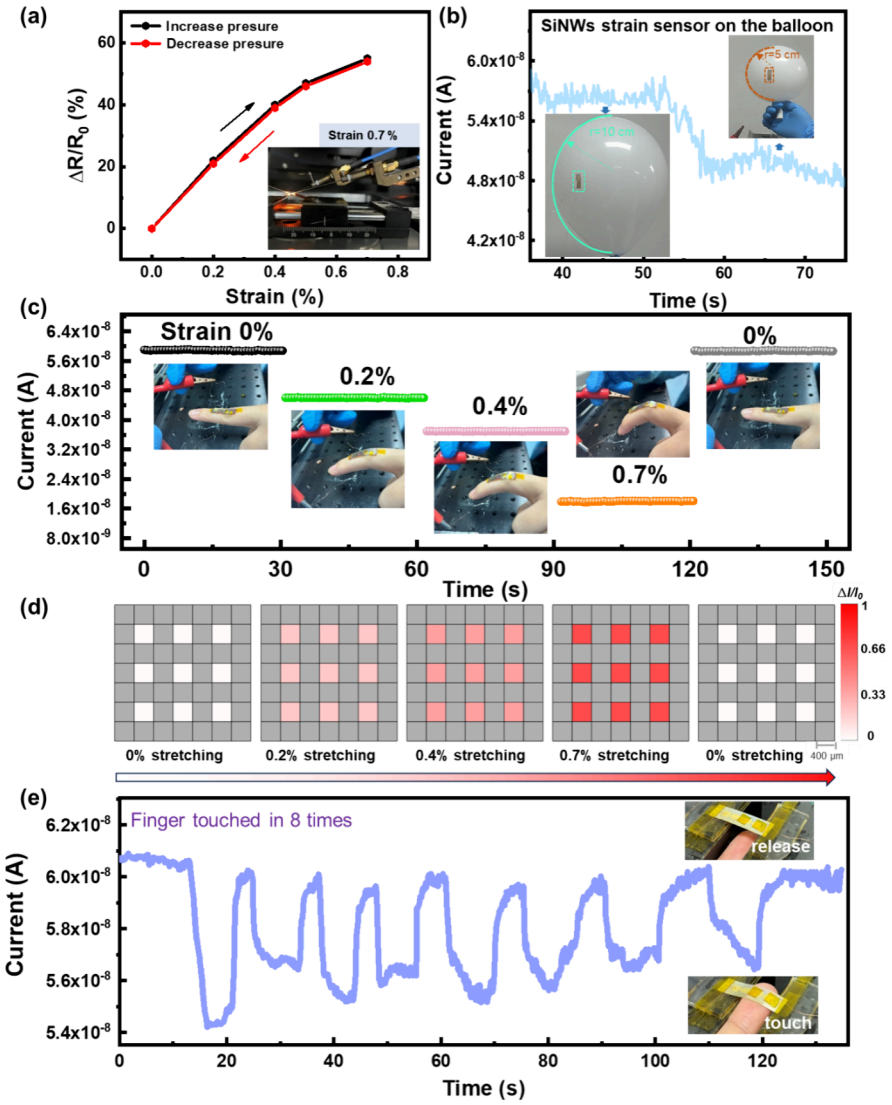

Figure 4. (a) Resistance changes vs strain (0−0.7%) plot and hysteresis curve. (b-d) SiNW wearable strain sensor for detecting human joint motion and balloon strain: (b) Electrical response to balloon motion; (c) Current response to finger joint motion; (d) Normalized current mapping of a 3 × 3 SiNW sensor matrix under different stretches. (e) Real-time variation of the flexible strain sensor, inset shows the touch and release action.

nm, as statistically presented in Figure S2c. The structural property of SiNW was analyzed by using high resolution transmission electron microscopy (HR-TEM) in Figure S3, where the lattice fringes show an atomic spacing of approximately 3.14 Å, consistent with the standard atomic spacing among Si[111] planes.

Figure 3a shows a series of photographs of the flexible strain sensor, mounted on a stretching platform, under increasing stretching from initial state up to 3.3% strain. spring-shaped SiNWs can withstand up to 3.3% strain without significant fracture and maintain good electrical contact. Figure 3b presents the electrical characteristics curve of the sensor during the straining process. The In atom concentration dissolved in the SiNW grown by the IPSLS mechanism can reach up to $\sim 10^{19}$ cm^{-3}.[40] When the SiNWs form an Ohmic contact with Pt/Au, the current gradually decreases as the strain increases. This is a characteristic result of the tensile stress-induced changes in p-type SiNWs.[41] As the strain increases gradually from 0% to 3.3%, the conductivity decreases from 0.98 S/cm to 0.08 S/cm (Figure S4). Under tensile stress, the length of the spring-shaped SiNWs increases, which leads to a significant increase in resistance. Tensile stress changes the lattice constant, distorts the band structure, and increases the effective mass of holes, all of which contribute to further increasing resistance. Additionally, tensile stress increases the defect density, creating more scattering centers that hinder hole transport.[42,43] Figure 3c shows that the current gradually decreases as the strain increases. In comparison, the straight-shaped SiNWs strain sensor fails, as illustrated in Figure S 2d, once the strain reaches 1%, owing to the fracture of the NWs (Figure S5).

Then, we investigated the sensitivity of the device. The gauge factor (GF), which represents the strain sensitivity, is defined as the ratio of the change in resistance to the change in length. $GF = (\Delta R/R_0)/(\Delta L/L_0) = (\Delta R/R_0)/\varepsilon$. ΔR and R are resistance change and original resistance, respectively. ΔL and L are length change and original length, respectively. ε is the applied strain.[18] Figure 3d illustrates the change in resistance variation from fast to slow as the strain gradually increases. After extracting the GF values, it was found that under smaller strains (0−0.8%), the resistance change exhibits a clear linear relationship, with a GF value as high as 86.3. This is

https://doi.org/10.1021/acs.nanolett.4c05553
Nano Lett. 2025, 25, 2290−2297

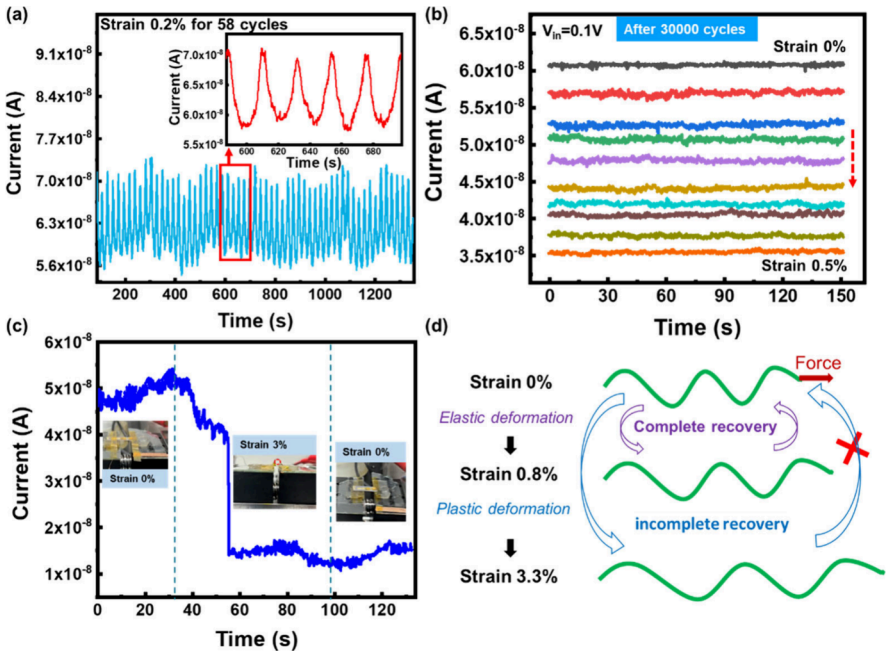

Figure 5. (a) Current response over 58 cycles of 0.2% strain, inset shows an enlargement of 5 cycles. (b) Sensor response to different strain levels (0−0.5%) after 30,000 cycles of 0.2% strain. (c) Current response of the sensor from its initial state, through 3% strain, and back to the initial state. (d) Schematic of the nanowire's deformation from 0% to 0.8% to 3.3% strain.

significantly higher than the GF for bulk silicon, indicating better strain sensitivity. The GF values in this range are also higher than those reported for other SiNWs, nanoribbons, and nanorods.[13,29,44−46] However, as the strain increases to 3.3%, the GF value drops to 9.1. This variation is primarily due to elastic deformation before 0.8% strain, followed by plastic deformation (0.8%−3.3%). We tested and statistically analyzed 15 devices from their initial state up to 0.5% strain, indicating good uniformity and reliability. Similar trends were observed in flexible strain sensors made from spring-shaped NWs with finer diameters (∼80 nm), as shown in Figure S6. The resistance changes in the 0−0.5% strain range show a good linear relationship, with a GF value reaching 91.2, validating the high strain sensitivity of the sensors.

Furthermore, during the strain process up to 0.7%, almost no hysteresis was observed in the forward and reverse scans of resistance change, as shown in Figure 4a, demonstrating the excellent stability and reliability of the flexible strain sensor. To demonstrate the application on a complex surface, the sensor was attached to a balloon and connected to a source meter via copper wires. As the balloon's curvature radius changed from ∼10 cm (0.05% strain) to 5 cm (0.1% strain), the electrical signals in Figure 4b show a gradual decrease, indicating reliable operation on complex surfaces. Additionally, the SiNWs were used as wearable sensors by attaching the strain sensor to a finger, with copper wires bonded to the electrodes and connected externally with alligator clips, creating a wearable finger joint motion sensor (Figure 4c). The sensor exhibits excellent flexibility, high sensitivity, and outstanding repeatability in response to finger joint movements, corresponding to strains of 0−0.7%. To illustrate the effect of strain on current changes, we plotted a 3 × 3 matrix under varying strains (Figure 4d). With increasing strain, the color indicative of current changes became more intense, and the array demonstrated reversible behavior upon returning the strain to its initial state. Figure 4e shows the real-time current variation during continuous touching and releasing of the sensor by a finger, illustrating excellent flexibility. The simulation data (Figure S7) showed excellent linearity for strains between 0 and 0.8% and a broad detection range from 0 to 490 MPa, which is significantly wider compared to similar flexible silicon-based strain sensors (typically up to several kPa).

In addition, the durability of the strain sensor was investigated within the strain range of 0% to 0.2%. Figure 5a shows the real-time current response over 58 cycles at 0.2% strain, with the inset providing an enlarged view of 5 cycles, demonstrating excellent recovery. After 30,000 cycles at 0.2% strain, the device still exhibits high stability and repeatability. As shown in Figure 5b, the electrical performance of the device from 0% to 0.5% strain after 30,000 cycles remains comparable to its initial state, as depicted in Figure 3c. To further examine the current response and repeatability of the sensor under high strain, we conducted a single tensile cycle from 0% to 3% and back to 0%. The real-time current change curve is recorded in Figure 5c. The results indicate that under high strain, the device almost fails to return to its initial current state but still maintains good electrical contact, as explained by the elastic and plastic deformation,[47] as shown in Figure 5d. The SiNWs typically exhibit a significant piezoresistive effect under stress. In contrast to bulk silicon, which usually exhibits brittleness at room temperature due to the high Peierls stress required for dislocation nucleation and/or motion, only at a considerable fraction of their melting point can dislocations be activated, allowing the material to become ductile. It has been reported that the necessary temperature for triggering plastic deformation in bulk silicon under stress is at least 400 °C.[48] This means that bulk silicon hardly undergoes plastic deformation at room temperature. However, when the material size is reduced to the nanoscale, nanomaterials can withstand high fracture stresses, which may eventually allow them to overcome the

https://doi.org/10.1021/acs.nanolett.4c05553
Nano Lett. 2025, 25, 2290−2297

Table 1. Comparison of the SiNW Strain Sensors to the Other Flexible/Stretchable Sensors

Materials	Fabrication strategies	Channel Length (L) and Width (W)	Substrate materials	Equal tensile range (%)	Gauge factor	Detection range	Stability (cycle)	refs.
(PU−PDMS) nanomeshes	Electrospinning and Transfer	L = 3 mm W = 8 mm	PDMS 200 μm	0−60	46.3		60% strain for 5000 cycles	18
PiI2T-Si thin film polymer	Solution and Spin-coating	L = 40 μm W ∼ 12 mm	PI 12 μm			0−8 KPa	15000	20
Pt-coated polymeric nanofibres	Solution etching and Transfer	L = 4 cm W = 5 cm	PDMS 500 μm	0−2	11. 45	5−1.5 KPa	10000	53
PDMS/CNT Film	Solution and Spin-coating	L = 100 μm W = 100 μm	PI 50 μm	0−0.3	∼33.33	10−100 KPa	100 KPa for 1000 cycles	54
Graphene Nanosheets	Solution	L ∼ 3 cm[a] W ∼ 3 cm[a]	PDMS			0−3.4 KPa	10000	55
Ag Nanowire	Solution and Spin-coating	L ∼ 100 μm[a] W ∼ 1 mm[a]	PDMS 100 μm	0−50	∼0.04	0−100 KPa	10000	23
Galinstan-Nickle composite	Solution and Printing	L ∼ 100 μm[a] W ∼ 1 mm[a]	PDMS 1000 μm	0−200	∼16.15			56
Silicon nanomembrane	SOI etching and Transfer	L ∼ 500 μm[a] W ∼ 1 mm[a]	PI 1.2 μm	0−15	0.5			45
Silicon Nanoribbons	SOI etching and Transfer	L = 200 μm W = 20 μm	PI 75 μm	1	43		1000	46
Silicon nanorod arrays	MACE etching	L = 16 mm W = 16 mm	PI/PDMS		∼45	0−3 KPa 3−170 KPa	1000	44
Single SiNW	VLS and Transfer	L = ∼5 mm[a] W ∼ 500 nm	PDMS 100 μm	0−0.22	∼1		>10000	13
Single SiNW	VLS& Transfer	L = 2 cm W ∼ 500 nm	PET	0−0.08	52		100	33
Self-aligned SiNWs/ Spring	IPSLS growth	L = 3 μm W ∼ 10[a]−150 nm	PI 100 μm	0−0.8	86.3	0−490 MPa	Strain 0.2% for 30000 cycles	This work

[a]Values estimated from the plots or graphs in the references.

critical resolved shear stress and nucleate ductile dislocations or make these dislocations mobile.[49]

When SiNWs are subjected to tensile stress below their elastic limit, they undergo elastic deformation, with the crystal structure remaining intact and atoms experiencing minor displacements. Upon removing the external force, the atoms return to their original positions, allowing the nanowire to fully recover. This makes SiNWs exhibit good elasticity under small strains (0% to 0.8%). For even larger stretching, the spring-shaped SiNW sensors already demonstrate some kind of plasticity, as seen in Figure 5c, due to most likely the irreversible damage caused in the SiNW channels which are grounded on, and thus subject to the constraint of, the much harder PI foil surface.[49−51] Note that, the spring-shaped SiNWs alone are supposed to be able to accommodate much larger stretching, if they are not constrained by touch ground surface, as witnessed in our previous works.[33,52] To achieve a significantly larger detection range under stretching, the SiNWs can be released from the substrate surface and suspended above it, supported by two source/drain (S/D) electrode pads. We anticipate demonstrating large-strain sensors in our future work.

The performance of strain sensors made from spring-shaped SiNWs was compared with those materials (Table 1). These morphology-programmable SiNW strain sensors exhibit superior performance, operating stably under 0−0.8% strain with a high GF (∼90) and a broad detection range (0−740 MPa), alongside excellent durability (30,000 cycles). Importantly, they can be batch-produced at low temperatures on flexible substrates.

CONCLUSIONS

In this work, we demonstrate a reliable integration of high performance flexible SiNW strain sensor, where morphology-programmed SiNWs are directly grown on PI substrate and at predesigned locations via IPSLS mechanism. The SiNW sensor exhibits a high GF of ∼90, withstanding large tensile strains up to 3.3% for more than 30,000 cycles. These results indicate that high-performance c-Si nanoelectronic devices can be directly grown and integrated upon soft polymer substrates, enabling the development of a new generation of wearable/stretchable electronics, sensors, and displays with minimal manufacturing costs and excellent mechanical and electronic stability.

ASSOCIATED CONTENT

Supporting Information

The Supporting Information is available free of charge at https://pubs.acs.org/doi/10.1021/acs.nanolett.4c05553.

Schematic of the SiNW fabrication procedures and the IPSLS growth mechanism, SEM images of straight-shaped SiNWs; diameter statistics of high-density straight-shaped SiNWs directly grown on a flexible PI substrate and typical electrical characteristic of the straight-shaped NW during the straining process, TEM of a SiNW segment grown at 200 °C, with a HR-TEM lattice image, conductivity under different strain conditions, SEM image of straight-shaped NW fracturing at 1% strain, optical images and device performance of strain sensors prepared using spring-shaped NWs (with finer diameters) directly grown on a PI substrate, the

https://doi.org/10.1021/acs.nanolett.4c05553
Nano Lett. 2025, 25, 2290−2297

stress−$\Delta R/R_0$ relationship curves for the top and bottom ends of spring-shaped nanowire (PDF)

AUTHOR INFORMATION

Corresponding Authors

Linwei Yu − *School of Electronics Science and Engineering, Nanjing University, 210023 Nanjing, P. R. China;* orcid.org/0000-0002-0801-5210; Email: yulinwei@nju.edu.cn

Sheng Wang − *School of Future Science and Engineering, Soochow University, 215222 Suzhou, P. R. China;* Email: shengwang@suda.edu.cn

Authors

Xiaopan Song − *School of Electronics Science and Engineering, Nanjing University, 210023 Nanjing, P. R. China*

Yang Gu − *School of Future Science and Engineering, Soochow University, 215222 Suzhou, P. R. China*

Junyu Fan − *School of Future Science and Engineering, Soochow University, 215222 Suzhou, P. R. China*

Junyang An − *School of Electronics Science and Engineering, Nanjing University, 210023 Nanjing, P. R. China;* orcid.org/0009-0008-2522-5165

Lei Yan − *School of Electronics Science and Engineering, Nanjing University, 210023 Nanjing, P. R. China;* orcid.org/0000-0002-6776-2400

Bin Sun − *School of Future Science and Engineering, Soochow University, 215222 Suzhou, P. R. China*

Junzhuan Wang − *School of Electronics Science and Engineering, Nanjing University, 210023 Nanjing, P. R. China*

Complete contact information is available at: https://pubs.acs.org/10.1021/acs.nanolett.4c05553

Notes

The authors declare no competing financial interest.

ACKNOWLEDGMENTS

The authors acknowledge the financial supports received from the Fundamental Research Funds for the Central Universities, the National Key Research Program of China under granted No. 92164201, National Natural Science Foundation of China for Distinguished Young Scholars No. 62325403, Natural Science Foundation of Jiangsu Province (BK20230498), Jiangsu Funding Program for Excellent Postdoctoral Talent (2024ZB427), the National Natural Science Foundation of China (61934004), and the National Natural Science Foundation of China (62304147).

REFERENCES

(1) Wang, C.; Xia, K.; Wang, H.; Liang, X.; Yin, Z.; Zhang, Y. Advanced Carbon for Flexible and Wearable Electronics. *Adv. Mater.* **2019**, *31*, No. e1801072.

(2) Lee, J. H.; Cho, K.; Kim, J. K. Age of Flexible Electronics: Emerging Trends in Soft Multifunctional Sensors. *Adv. Mater.* **2024**, *36*, No. e2310505.

(3) Hua, Q.; Shen, G. Low-dimensional nanostructures for monolithic 3D-integrated flexible and stretchable electronics. *Chem. Soc. Rev.* **2024**, *53*, 1316−1353.

(4) Gong, S.; Lu, Y.; Yin, J.; Levin, A.; Cheng, W. Materials-Driven Soft Wearable Bioelectronics for Connected Healthcare. *Chem. Rev.* **2024**, *124*, 455−553.

(5) Arwani, R. T.; Tan, S. C. L.; Sundarapandi, A.; Goh, W. P.; Liu, Y.; Leong, F. Y.; Yang, W.; Zheng, X. T.; Yu, Y.; Jiang, C.; Ang, Y. C.; Kong, L.; Teo, S. L.; Chen, P.; Su, X.; Li, H.; Liu, Z.; Chen, X.; Yang, L.; Liu, Y. Stretchable ionic-electronic bilayer hydrogel electronics enable in situ detection of solid-state epidermal biomarkers. *Nat. Mater.* **2024**, *23*, 1115−1122.

(6) Li, G.; Ma, Z.; You, C.; Huang, G.; Song, E.; Pan, R.; Zhu, H.; Xin, J.; Xu, B.; Lee, T.; et al. Silicon nanomembrane phototransistor flipped with multifunctional sensors toward smart digital dust. *Sci. Adv.* **2020**, *6*, eaaz6511.

(7) Khan, Y.; Thielens, A.; Muin, S.; Ting, J.; Baumbauer, C.; Arias, A. C. A New Frontier of Printed Electronics: Flexible Hybrid Electronics. *Adv. Mater.* **2020**, *32*, No. e1905279.

(8) Zhong, D.; Wu, C.; Jiang, Y.; Yuan, Y.; Kim, M.-g.; Nishio, Y.; Shih, C.-C.; Wang, W.; Lai, J.-C.; Ji, X.; Gao, T. Z.; Wang, Y.-X.; Xu, C.; Zheng, Y.; Yu, Z.; Gong, H.; Matsuhisa, N.; Zhao, C.; Lei, Y.; Liu, D.; Zhang, S.; Ochiai, Y.; Liu, S.; Wei, S.; Tok, J. B. H.; Bao, Z. Author Correction: High-speed and large-scale intrinsically stretchable integrated circuits. *Nature* **2024**, *630*, E12−E12.

(9) Li, W. D.; Ke, K.; Jia, J.; Pu, J. H.; Zhao, X.; Bao, R. Y.; Liu, Z. Y.; Bai, L.; Zhang, K.; Yang, M. B.; Yang, W. Recent Advances in Multiresponsive Flexible Sensors towards E-skin: A Delicate Design for Versatile Sensing. *Small* **2022**, *18*, No. e2103734.

(10) Cheng, W.; Wang, X.; Xiong, Z.; Liu, J.; Liu, Z.; Jin, Y.; Yao, H.; Wong, T. S.; Ho, J. S.; Tee, B. C. K. Frictionless multiphasic interface for near-ideal aero-elastic pressure sensing. *Nat. Mater.* **2023**, *22*, 1352−1360.

(11) Fu, X.; Cheng, W.; Wan, G.; Yang, Z.; Tee, B. C. K. Toward an AI Era: Advances in Electronic Skins. *Chem. Rev.* **2024**, *124*, 9899−9948.

(12) Shi, Y.; Zhao, J.; Zhang, B.; Qin, J.; Hu, X.; Cheng, Y.; Yu, J.; Jie, J.; Zhang, X. Freestanding Serpentine Silicon Strips with Ultrahigh Stretchability over 300% for Wearable Electronics. *Adv. Mater.* **2024**, *36*, No. e2313603.

(13) Huang, S.; Zhang, B.; Shao, Z.; He, L.; Zhang, Q.; Jie, J.; Zhang, X. Ultraminiaturized Stretchable Strain Sensors Based on Single Silicon Nanowires for Imperceptible Electronic Skins. *Nano Lett.* **2020**, *20*, 2478−2485.

(14) Tang, N.; Zhou, C.; Qu, D.; Fang, Y.; Zheng, Y.; Hu, W.; Jin, K.; Wu, W.; Duan, X.; Haick, H. A Highly Aligned Nanowire-Based Strain Sensor for Ultrasensitive Monitoring of Subtle Human Motion. *Small* **2020**, *16*, No. 2001363.

(15) Peng, S.; Wang, Z.; Lin, J.; Miao, J. T.; Zheng, L.; Yang, Z.; Weng, Z.; Wu, L. Tailored and Highly Stretchable Sensor Prepared by Crosslinking an Enhanced 3D Printed UV-Curable Sacrificial Mold. *Adv. Funct. Mater.* **2021**, *31*, 2008729.

(16) Kim, J.; Lee, M.; Shim, H. J.; Ghaffari, R.; Cho, H. R.; Son, D.; Jung, Y. H.; Soh, M.; Choi, C.; Jung, S.; Chu, K.; Jeon, D.; Lee, S. T.; Kim, J. H.; Choi, S. H.; Hyeon, T.; Kim, D. H. Stretchable silicon nanoribbon electronics for skin prosthesis. *Nat. Commun.* **2014**, *5*, 5747.

(17) Yamada, T.; Hayamizu, Y.; Yamamoto, Y.; Yomogida, Y.; Izadi-Najafabadi, A.; Futaba, D. N.; Hata, K. A stretchable carbon nanotube strain sensor for human-motion detection. *Nat. Nanotechnol* **2011**, *6*, 296−301.

(18) Wang, Y.; Lee, S.; Yokota, T.; Wang, H.; Jiang, Z.; Wang, J.; Koizumi, M.; Someya, T. A durable nanomesh on-skin strain gauge for natural skin motion monitoring with minimum mechanical constraints. *Sci. Adv.* **2020**, *6*, eabb7043.

(19) Qiu, A.; Li, P.; Yang, Z.; Yao, Y.; Lee, I.; Ma, J. A Path Beyond Metal and Silicon:Polymer/Nanomaterial Composites for Stretchable Strain Sensors. *Adv. Funct. Mater.* **2019**, *29*, 1806306.

(20) Schwartz, G.; Tee, B. C.; Mei, J.; Appleton, A. L.; Kim, D. H.; Wang, H.; Bao, Z. Flexible polymer transistors with high pressure sensitivity for application in electronic skin and health monitoring. *Nat. Commun.* **2013**, *4*, 1859.

(21) Lin, Y.; Fang, T.; Bai, C.; Sun, Y.; Yang, C.; Hu, G.; Guo, H.; Qiu, W.; Huang, W.; Wang, L.; Tao, Z.; Lu, Y. Q.; Kong, D. Ultrastretchable Electrically Self-Healing Conductors Based on Silver

Nanowire/Liquid Metal Microcapsule Nanocomposites. *Nano Lett.* **2023**, *23*, 11174−11183.
(22) Gong, S.; Zhang, X.; Nguyen, X. A.; Shi, Q.; Lin, F.; Chauhan, S.; Ge, Z.; Cheng, W. Hierarchically resistive skins as specific and multimetric on-throat wearable biosensors. *Nat. Nanotechnol.* **2023**, *18*, 889−897.
(23) Han, J.; Yang, J.; Gao, W.; Bai, H. Ice-Templated, Large-Area Silver Nanowire Pattern for Flexible Transparent Electrode. *Adv. Funct. Mater.* **2021**, *31*, 2010155.
(24) Dong, T.; Sun, Y.; Zhu, Z.; Wu, X.; Wang, J.; Shi, Y.; Xu, J.; Chen, K.; Yu, L. Monolithic Integration of Silicon Nanowire Networks as a Soft Wafer for Highly Stretchable and Transparent Electronics. *Nano Lett.* **2019**, *19*, 6235−6243.
(25) Zhang, B. C.; Wang, H.; Zhao, Y.; Li, F.; Ou, X. M.; Sun, B. Q.; Zhang, X. H. Large-scale assembly of highly sensitive Si-based flexible strain sensors for human motion monitoring. *Nanoscale* **2016**, *8*, 2123−2128.
(26) Lin, S.; Liu, J.; Li, W.; Wang, D.; Huang, Y.; Jia, C.; Li, Z.; Murtaza, M.; Wang, H.; Song, J.; Liu, Z.; Huang, K.; Zu, D.; Lei, M.; Hong, B.; Wu, H. A Flexible, Robust, and Gel-Free Electroencephalogram Electrode for Noninvasive Brain-Computer Interfaces. *Nano Lett.* **2019**, *19*, 6853−6861.
(27) Chan, C. K.; Peng, H.; Liu, G.; McIlwrath, K.; Zhang, X. F.; Huggins, R. A.; Cui, Y. High-performance lithium battery anodes using silicon nanowires. *Nat. Nanotechnol* **2008**, *3*, 31−35.
(28) Zhang, H.; Xu, H.; Xiao, Z.; Dong, G.; Cheng, Y.; Fei, F.; Hu, X.; Xu, L.; Mai, L. Nanowires for Solid-State Lithium Batteries. *Adv. Funct. Mater.* **2024**, *35*, No. 2412548.
(29) Zhang, B. C.; Wang, H.; He, L.; Zheng, C. J.; Jie, J. S.; Lifshitz, Y.; Lee, S. T.; Zhang, X. H. Centimeter-Long Single-Crystalline Si Nanowires. *Nano Lett.* **2017**, *17*, 7323−7329.
(30) Song, X.; Wu, L.; Liang, Y.; Liu, Z.; Wang, J.; Xu, J.; Chen, K.; Yu, L. High-Performance Transparent Silicon Nanowire Thin Film Transistors Integrated on Glass Substrates via a Room Temperature Solution Passivation. *Adv. Electron. Mater.* **2023**, *9*, 2201236.
(31) Song, X.; Zhang, T.; Wu, L.; Hu, R.; Qian, W.; Liu, Z.; Wang, J.; Shi, Y.; Xu, J.; Chen, K.; Yu, L. Highly Stretchable High-Performance Silicon Nanowire Field Effect Transistors Integrated on Elastomer Substrates. *Adv. Sci.* **2022**, *9*, No. e2105623.
(32) Song, X.; Hu, R.; Xu, S.; Liu, Z.; Wang, J.; Shi, Y.; Xu, J.; Chen, K.; Yu, L. Highly Sensitive Ammonia Gas Detection at Room Temperature by Integratable Silicon Nanowire Field-Effect Sensors. *ACS Appl. Mater. Interfaces* **2021**, *13*, 14377−14384.
(33) Xue, Z.; Sun, M.; Dong, T.; Tang, Z.; Zhao, Y.; Wang, J.; Wei, X.; Yu, L.; Chen, Q.; Xu, J.; et al. Deterministic Line-Shape Programming of Silicon Nanowires for Extremely Stretchable Springs and Electronics. *Nano Lett.* **2017**, *17*, 7638−7646.
(34) Yu, L.; Chen, W.; O'Donnell, B.; Patriarche, G.; Bouchoule, S.; Pareige, P.; Rogel, R.; Claire Salaun, A.; Pichon, L.; Roca i Cabarrocas, P. Growth-in-place deployment of in-plane silicon nanowires. *Appl. Phys. Lett.* **2011**, *99*, 203104.
(35) Yu, L.; i Cabarrocas, P. R. Growth mechanism and dynamics of in-plane solid-liquid-solid silicon nanowires. *Phys. Rev. B* **2010**, *81*, No. 085323.
(36) Yu, L.; Oudwan, M.; Moustapha, O.; Fortuna, F.; Roca i Cabarrocas, P. Guided growth of in-plane silicon nanowires. *Appl. Phys. Lett.* **2009**, *95*, 113106.
(37) Zhang, H.; Tersoff, J.; Xu, S.; Chen, H.; Zhang, Q.; Zhang, K.; Yang, Y.; Lee, C. S.; Tu, K. N.; Li, J.; Lu, Y. Approaching the ideal elastic strain limit in silicon nanowires. *Sci. Adv.* **2016**, *2*, No. e1501382.
(38) Minamisawa, R. A.; Süess, M. J.; Spolenak, R.; Faist, J.; David, C.; Gobrecht, J.; Bourdelle, K. K.; Sigg, H. Top-down fabricated silicon nanowires under tensile elastic strain up to 4.5%. *Nat. Commun.* **2012**, *3*, 1096.
(39) Minoshima, K.; Terada, T.; Komai, K. Influence of nanometre-sized notch and water on the fracture behaviour of single crystal silicon microelements. *Fatigue Fract. Eng. M.* **2000**, *23*, 33−104.
(40) Chen, W.; Yu, L.; Misra, S.; Fan, Z.; Pareige, P.; Patriarche, G.; Bouchoule, S.; Cabarrocas, P. R. i Incorporation and redistribution of impurities into silicon nanowires during metal-particle-assisted growth. *Nat. Commun.* **2014**, *5*, 4134.
(41) Yin, H.; Yang, H.; Xu, S.; Pan, D.; Xu, J.; Chen, K.; Yu, L. High Performance Si Nanowire TFTs With Ultrahigh on/off Current Ratio and Steep Subthreshold Swing. *IEEE Electron Device Lett.* **2020**, *41*, 46−49.
(42) Milne, J. S.; Rowe, A. C.; Arscott, S.; Renner, C. Giant piezoresistance effects in silicon nanowires and microwires. *Phys. Rev. Lett.* **2010**, *105*, 226802.
(43) He, R.; Yang, P. Giant piezoresistance effect in silicon nanowires. *Nat. Nanotechnol* **2006**, *1*, 42−46.
(44) Ghosh, R.; Song, M. S.; Park, J.; Tchoe, Y.; Guha, P.; Lee, W.; Lim, Y.; Kim, B.; Kim, S.-W.; Kim, M.; Yi, G.-C. Fabrication of piezoresistive Si nanorod-based pressure sensor arrays: A promising candidate for portable breath monitoring devices. *Nano Energy* **2021**, *80*, No. 105537.
(45) Son, D.; Lee, J.; Qiao, S.; Ghaffari, R.; Kim, J.; Lee, J. E.; Song, C.; Kim, S. J.; Lee, D. J.; Jun, S. W.; Yang, S.; Park, M.; Shin, J.; Do, K.; Lee, M.; Kang, K.; Hwang, C. S.; Lu, N.; Hyeon, T.; Kim, D. H. Multifunctional wearable devices for diagnosis and therapy of movement disorders. *Nat. Nanotechnol* **2014**, *9*, 397−404.
(46) Won, S. M.; Kim, H.-S.; Lu, N.; Kim, D.-G.; Del Solar, C.; Duenas, T.; Ameen, A.; Rogers, J. A. Piezoresistive Strain Sensors and Multiplexed Arrays Using Assemblies of Single-Crystalline Silicon Nanoribbons on Plastic Substrates. *IEEE Trans. Electron Devices* **2011**, *58*, 4074−4078.
(47) Wang, S.; Shan, Z.; Huang, H. The Mechanical Properties of Nanowires. *Adv. Sci.* **2017**, *4*, 1600332.
(48) George, A.; Yip, S. Preface to the Viewpoint Set on:: Dislocation mobility in silicon. *Scr. Mater.* **2001**, *45*, 1233−1238.
(49) Zheng, K.; Han, X.; Wang, L.; Zhang, Y.; Yue, Y.; Qin, Y.; Zhang, X.; Zhang, Z. Atomic mechanisms governing the elastic limit and the incipient plasticity of bending Si nanowires. *Nano Lett.* **2009**, *9*, 2471−2476.
(50) Tang, D. M.; Ren, C. L.; Wang, M. S.; Wei, X.; Kawamoto, N.; Liu, C.; Bando, Y.; Mitome, M.; Fukata, N.; Golberg, D. Mechanical properties of Si nanowires as revealed by in situ transmission electron microscopy and molecular dynamics simulations. *Nano Lett.* **2012**, *12*, 1898−1904.
(51) Wang, L.; Zheng, K.; Zhang, Z.; Han, X. Direct atomic-scale imaging about the mechanisms of ultralarge bent straining in Si nanowires. *Nano Lett.* **2011**, *11*, 2382−2385.
(52) Yuan, R.; Qian, W.; Liu, Z.; Wang, J.; Xu, J.; Chen, K.; Yu, L. Designable Integration of Silicide Nanowire Springs as Ultra-Compact and Stretchable Electronic Interconnections. *Small* **2022**, *18*, No. e2104690.
(53) Pang, C.; Lee, G. Y.; Kim, T. I.; Kim, S. M.; Kim, H. N.; Ahn, S. H.; Suh, K. Y. A flexible and highly sensitive strain-gauge sensor using reversible interlocking of nanofibres. *Nat. Mater.* **2012**, *11*, 795−801.
(54) Ma, C.; Xu, D.; Huang, Y. C.; Wang, P.; Huang, J.; Zhou, J.; Liu, W.; Li, S. T.; Huang, Y.; Duan, X. Robust Flexible Pressure Sensors Made from Conductive Micropyramids for Manipulation Tasks. *ACS Nano* **2020**, *14*, 12866−12876.
(55) Li, Y.; Cui, Y.; Zhang, M.; Li, X.; Li, R.; Si, W.; Sun, Q.; Yu, L.; Huang, C. Ultrasensitive Pressure Sensor Sponge Using Liquid Metal Modulated Nitrogen-Doped Graphene Nanosheets. *Nano Lett.* **2022**, *22*, 2817−2825.
(56) Chen, P.; Zhou, X. P. Biphasic Liquid Metal Composite for Strain Sensor with High Stretchability and Sensitivity. *Adv. Eng. Mater.* **2024**, *26*, 2400211.

https://doi.org/10.1021/acs.nanolett.4c05553
Nano Lett. 2025, 25, 2290−2297